Sol-gel preparation of a novel $\chi La_2Ti_2O_7$/HZSM-5 composite photocatalyst

WENJIE ZHANG*, YUXUAN LIU, LING DU
School of Environmental and Chemical Engineering, Shenyang Ligong University, Shenyang 110159, China

A sol-gel method was used to prepare $\chi La_2Ti_2O_7$/HZSM-5 composite using HZSM-5 zeolite as the support. $La_2Ti_2O_7$ is in the layered-perovskite structure after loading. Crystallite size of $La_2Ti_2O_7$ shrinks slightly with decreasing loading percentage. Surface area and total pore volume of $\chi La_2Ti_2O_7$/HZSM-5 significantly increase with raising HZSM-5 content. The bandgap energies are 3.29, 3.55, 3.61, 3.63 and 3.73 eV for bare $La_2Ti_2O_7$ and the composites containing 90%, 70%, 50% and 20% $La_2Ti_2O_7$. The chemical environments of La, Ti and O in $La_2Ti_2O_7$ do not noticeably change after loading. 34.8% of the initial RBR-X3B is degraded on 70%$La_2Ti_2O_7$/HZSM-5 after 30 min of irradiation, while only 6.4% of the dye is degraded on the bare $La_2Ti_2O_7$.

(Received January 11, 2017; accepted April 5, 2018)

Keywords: $La_2Ti_2O_7$, Photocatalytic, HZSM-5, Support

1. Introduction

Photocatalytic technique is one of the most studied environmental cleaning techniques in the past decades [1-3]. The most focused research topics in this field are about developments of new photocatalytic materials and preparation methods [4-6]. Inorganic titanate materials in perovskite structure are potential photocatalytic materials in industrial applications due to high mobilization of charge carriers and the band structure for visible light response [7-11].

In order to improve photocatalytic activity to facilitate removing efficiency of environmental pollutants, many modification techniques such as metal doping, composite material and supporting are used. Supporting is considered to be an effective modification technique in the purpose of improving photocatalytic activity in pollutant treatment. Zeolite is one of the important supports in this research. The superiorities of using zeolite as the support are not only the high specific surface, but also the ability in controlling charge transfer [12].

$La_2Ti_2O_7$ is reported as a potential photocatalyst due to its high photoelectric conversion efficiency and thermal stability [13]. It has been applied to work for various purposes in the photocatalysis field [14-16]. However, photocatalytic activity of $La_2Ti_2O_7$ is weak because the material usually has large crystal size (more than hundreds of nanometers) and small specific surface area (less than 10 m^2/g) [17]. Although HZSM-5 was applied to support TiO_2 and $SrTiO_3$ for promoted activity in our previous work [18,19], there is no literature concerning the use of HZSM-5 to support lanthanum titanate. In this work, $La_2Ti_2O_7$ was supported on HZSM-5 by a sol-gel method. The effects of $La_2Ti_2O_7$ loading content on properties of the $\chi La_2Ti_2O_7$/HZSM-5 composite were investigated.

2. Experimental

2.1. Synthesis of the materials

1.0825 g lanthanum nitrate was dissolved in 8 mL deionized water, followed by addition of 8 mL acetic acid. 0.85 mL tetrabutyl titanate was dissolved in 8 mL ethanol to form another solution. The two solutions were mixed together with the n(La)/n(Ti) molar ratio of 1:1. Subsequently, certain amount of HZSM-5 and 2 mL glycol were added into the former solution. The mixture was stirred to form a sticky gel. The gel was dried at 110 ^oC for 15 h, and calcined at 800 ^oC for 3 h. The solid was ground and denoted as $\chi La_2Ti_2O_7$/HZSM-5, where χ is the weight percentage of $La_2Ti_2O_7$ in the composite.

2.2. Characterization of the materials

Crystal structures of the materials were analyzed by D8 Advance X-ray diffractometer with Cu $K\alpha$ radiation (Tube voltage 40 kV, tube current 40 mA, scanning step 0.05 ^{o}/min, scanning speed 4 ^{o}/min). Chemical environment of elements was analyzed by ESCALAB 250Xi X-ray photoelectron spectroscopy (Al $K\alpha$, pass energy 100.0 eV, energy step 1.000 eV). Specific surface area and porous structure measurements were performed using a surface area and pore size analyzer (F-sorb 3400). The specific surface area was determined by the multipoint BET method. The desorption isotherm was used to determine pore size distribution using the Barrett, Joyner, and Halenda (BJH) method. An integrating sphere was set up on a LAMBDA 35 UV-Vis spectrometer to record UV-Vis diffuse reflectance spectra using $BaSO_4$ as a reference.

2.3. Photocatalytic activity

Photocatalytic activities of the materials were evaluated by degradation of Reactive Brilliant Red-X3B (RBR-X3B). 50 mL of 30 mg/L RBR-X3B solution and 25 mg $La_2Ti_2O_7$ were mixed in a 100 mL quartz reactor. The light source was a 20 W UV lamp that irradiated at wavelength of 253.7 nm. After the suspension reached adsorption-desorption equilibrium in the dark, the UV-light lamp was turned on to measure photocatalytic degradation efficiency. Absorbance of RBR-X3B solution was examined by a 721E spectrophotometer at the maximum absorption wavelength of 539 nm. RBR-X3B concentration was calculated according to Lambert-Beer theory.

3. Results and discussion

Fig. 1 shows the XRD patterns of $La_2Ti_2O_7$, $\chi La_2Ti_2O_7$/HZSM-5, and HZSM-5. The diffraction patterns of $La_2Ti_2O_7$ match well with the PDF card (JCPDS 81-1066), indicating a layered-perovskite $La_2Ti_2O_7$ synthesized in the sol-gel process without the production of any other phases of lanthanum titanate or impurities. The crystal phase of $La_2Ti_2O_7$ does not noticeably change after loading on HZSM-5. The crystallite size of $La_2Ti_2O_7$ at the preferred (-212) plane was calculated using Scherrer formula, $L=K\lambda/(\beta\cdot\cos\theta)$ [20-22]. L is the crystalline size, K is a dimensionless shape factor, λ is the X-ray wavelength, β is the line broadening at half the maximum intensity after subtracting the instrumental line broadening, and θ is the Bragg angle. Pure $La_2Ti_2O_7$ has a crystallite size of 23 nm, while the crystallite sizes of $La_2Ti_2O_7$ in 20%$La_2Ti_2O_7$/HZSM-5, 50%$La_2Ti_2O_7$/HZSM-5, 70% $La_2Ti_2O_7$/HZSM-5 and 90%$La_2Ti_2O_7$/HZSM-5 are 19, 21, 22 and 23 nm, respectively. Crystallite size of $La_2Ti_2O_7$ shrinks slightly with decreasing loading content, due to reducing crystal growth as the effect of $La_2Ti_2O_7$ dispersion on HZSM-5.

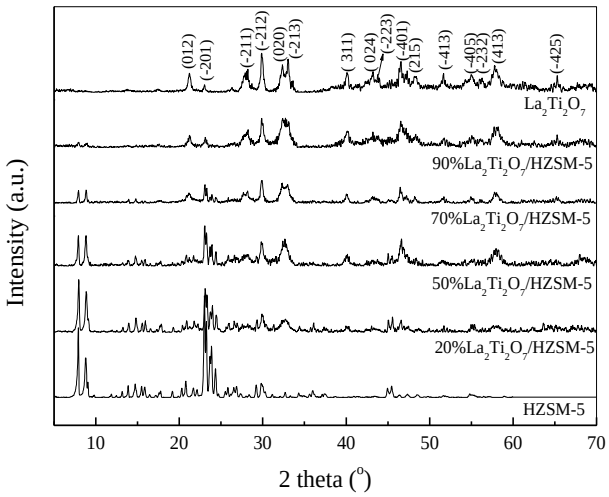

Fig. 1. XRD patterns of $La_2Ti_2O_7$, $\chi La_2Ti_2O_7$/HZSM-5, and HZSM-5

N_2 desorption isotherms of $La_2Ti_2O_7$ and $\chi La_2Ti_2O_7$/HZSM-5 with different loading content are shown in Fig. 2. The N_2 volume adsorbed on the materials are getting larger with decreasing $La_2Ti_2O_7$ loading content on the composites. The bare $La_2Ti_2O_7$ nearly has no adsorption capacity until the N_2 relative pressure is as high as 0.9. The enhancement of adsorbed N_2 volume on the supported composites is in accordance to the weight percent of HZSM-5 zeolite. All the desorption isotherms of the supported $\chi La_2Ti_2O_7$/HZSM-5 samples are classified as IUPAC type I for microporous material. The abrupt enlarged adsorption capacity at N_2 relative pressure over 0.9 is due to the interparticle macropores.

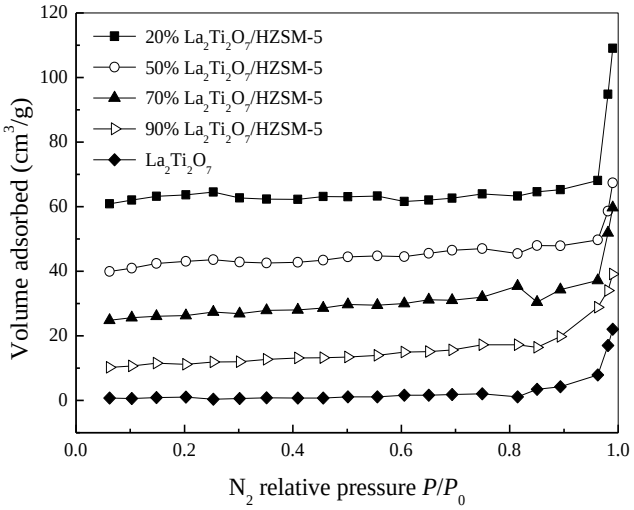

Fig. 2. N_2 desorption isotherms of $La_2Ti_2O_7$ and $\chi La_2Ti_2O_7$/HZSM-5 with different loading content

Table 1 also presents porous properties of $La_2Ti_2O_7$ and $\chi La_2Ti_2O_7$/HZSM-5. $La_2Ti_2O_7$ has a small surface area of 8.0 m^2/g. The very small pore volume of 0.0011 cm^3/g indicates a limited porous structure in $La_2Ti_2O_7$. Surface area and total pore volume of $\chi La_2Ti_2O_7$/HZSM-5 significantly go up with raising HZSM-5 content. The majorities of surface area and pore volume are contributed by the zeolite.

It's worth noting that pore volume of $\chi La_2Ti_2O_7$/HZSM-5 at low $La_2Ti_2O_7$ loading content (χ is between 20% and 50%) falls off with increasing $La_2Ti_2O_7$ content. However, the pore volume does not apparently decrease further at high $La_2Ti_2O_7$ loading content, due to formation of new mesopores inside the supported $La_2Ti_2O_7$.

Table 1. Crystallite sizes and porous properties of $La_2Ti_2O_7$ and $\chi La_2Ti_2O_7$/HZSM-5

Samples	Crystallite size (nm)	Surface area (m^2/g)	Average pore size (nm)	Pore volume (cm^3/g)
HZSM-5		223.8	1.9	0.11
20%$La_2Ti_2O_7$/HZSM-5	19	187.3	1.8	0.086
50%$La_2Ti_2O_7$/HZSM-5	21	128.2	1.8	0.057
70%$La_2Ti_2O_7$/HZSM-5	22	80.6	3.3	0.067
90%$La_2Ti_2O_7$/HZSM-5	23	36.2	6.1	0.055
$La_2Ti_2O_7$	23	8.0	0.6	0.0011

UV-Vis diffuse reflectance spectra of $La_2Ti_2O_7$ and $\chi La_2Ti_2O_7$/HZSM-5 with different loading content are measured, as shown in Fig. 3. Absorptions in the UV region below 300 nm by the $\chi La_2Ti_2O_7$/HZSM-5 composites are much larger than bare $La_2Ti_2O_7$ since HZSM-5 is almost insulative in UV and visible region. $La_2Ti_2O_7$ is direct allowed in electronic transition [15]. Bandgaps of $La_2Ti_2O_7$ and $\chi La_2Ti_2O_7$/HZSM-5 are calculated through Tauc plot, $(\alpha hv)^2 = A(hv-Eg)$ [23,24]. The bandgaps are 3.29, 3.55, 3.61, 3.63 and 3.73 eV for bare $La_2Ti_2O_7$ and the composites containing 90%, 70%, 50% and 20% $La_2Ti_2O_7$. A slight blue shift of the band edge can be seen with increasing HZSM-5 weight percent. This shift is mostly caused by the presence of HZSM-5 zeolite, while grain refining of $La_2Ti_2O_7$ after loading may also contribute to this effect.

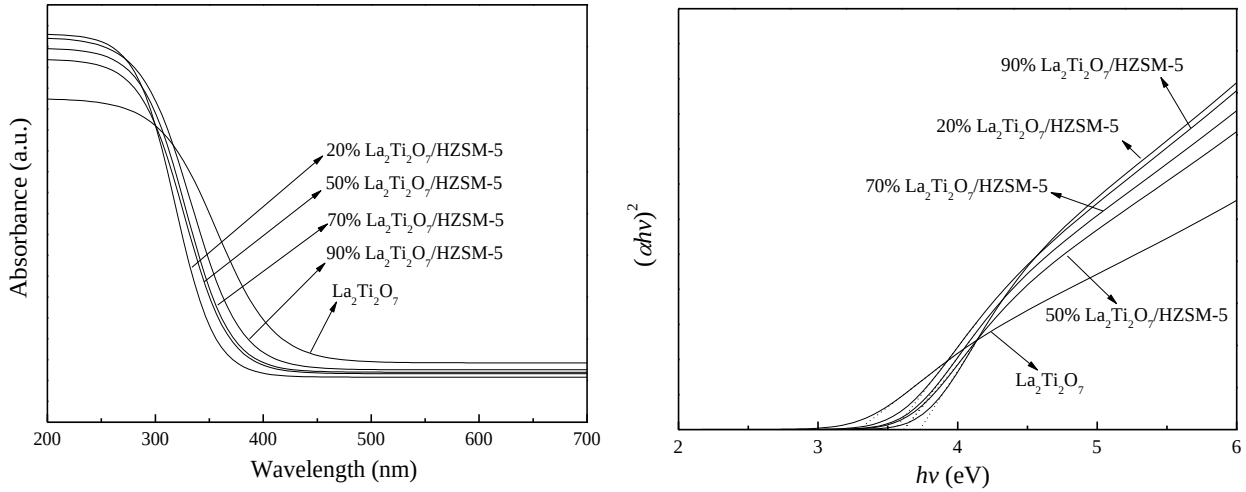

Fig. 3. UV-Vis diffuse reflectance spectra of $La_2Ti_2O_7$ and $\chi La_2Ti_2O_7$/HZSM-5 with different loading content

The XPS spectra of La3*d*, Ti2*p* and O1*s* regions for $La_2Ti_2O_7$ and 70%$La_2Ti_2O_7$/HZSM-5 are shown in Fig. 4. XPS PEAK Version 4.1 was used to perform the deconvolution of XPS profiles. La3*d* photoelectron peaks have strong shake-up satellites. The complex multi-peak structure in La3*d* core level is due to a spin–orbit interaction [25]. The binding energies of La3$d_{5/2}$ electrons in 70%$La_2Ti_2O_7$/HZSM-5 are 834.2, 836.0, 838.8 and 847.4 eV. The peaks at 851.0, 852.8, 855.6 and 862.7 eV are observed for La3$d_{3/2}$ electrons. The results show that La in 70%$La_2Ti_2O_7$/HZSM-5 is in trivalent states with oxide forming [26].

The two symmetrical peaks at 458.3 and 464.0 eV of Ti2*p* for 70%$La_2Ti_2O_7$/HZSM-5 are assigned to Ti2$p_{3/2}$ and Ti2$p_{1/2}$ electrons. The distance between Ti2$p_{3/2}$ and Ti2$p_{1/2}$ peaks is 5.7 eV, representing the characteristic Ti^{4+} state [27]. The binding energy peaks at 529.4, 529.7 and 531.3 eV are attributed to lattice oxygen, surface adsorbed oxygen, and hydroxyl in $La_2Ti_2O_7$ [5], respectively. Compared with O1*s* spectra of $La_2Ti_2O_7$, another peak of 70%$La_2Ti_2O_7$/HZSM-5 at 532.7 eV can be assigned to O in HZSM-5 [28]. The chemical environments of La, Ti and O in $La_2Ti_2O_7$ do not apparently change after loading. However, all the binding energies of La3*d*, Ti2*p* and O1*s* electrons in $La_2Ti_2O_7$ slightly increase after loading on HZSM-5, indicating a possible electron transfer from the coated $La_2Ti_2O_7$ to the HZSM-5 zeolite.

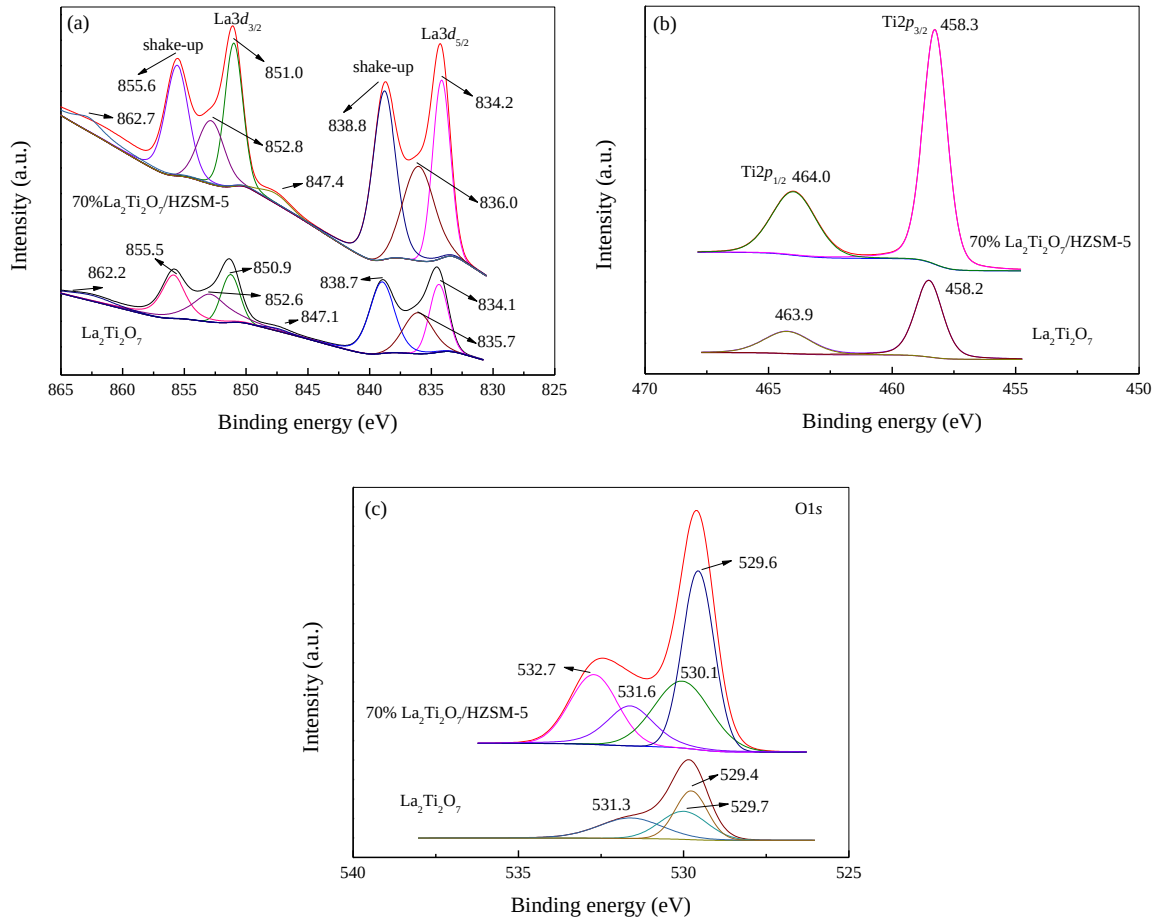

Fig. 4. XPS spectra of $La_2Ti_2O_7$ and 70%$La_2Ti_2O_7$/HZSM-5. (a) La3d, (b) Ti2p, (c) O1s

Fig. 5(a) shows photocatalytic degradation efficiency of RBR-X3B on χ$La_2Ti_2O_7$/HZSM-5. HZSM-5 has no photocatalytic activity in this work, and the bare $La_2Ti_2O_7$ has very weak photocatalytic activity. RBR-X3B degradation efficiency on χ$La_2Ti_2O_7$/HZSM-5 varies with the change of $La_2Ti_2O_7$ loading content. The maximum photocatalytic degradation efficiency is found on 70%$La_2Ti_2O_7$/HZSM-5. 34.8% of the initial RBR-X3B is degraded on 70%$La_2Ti_2O_7$/HZSM-5 after 30 min of irradiation, while only 6.4% of the dye is degraded on the bare $La_2Ti_2O_7$.

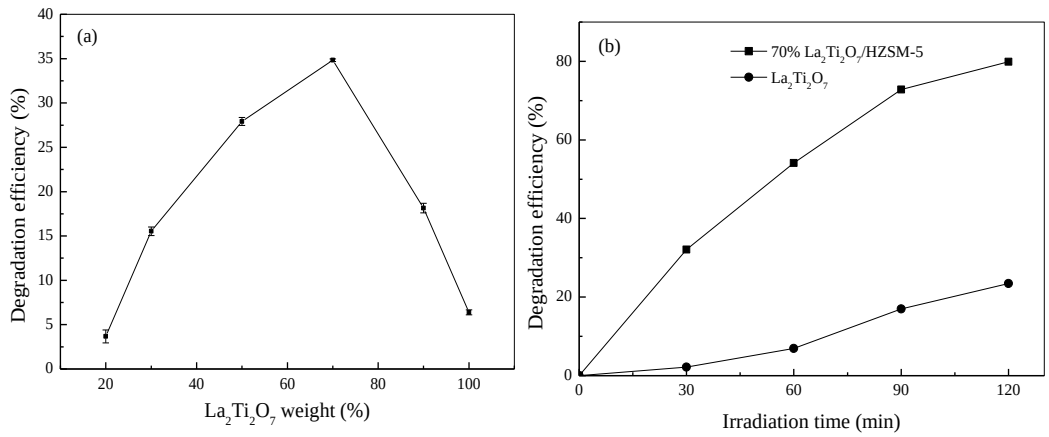

Fig. 5. (a) Photocatalytic degradation of RBR-X3B on χ$La_2Ti_2O_7$/HZSM-5 as the factor of loading content. The irradiation time was 30 min. (b) Comparison of photocatalytic degradation of RBR-X3B on $La_2Ti_2O_7$ and 70%$La_2Ti_2O_7$/HZSM-5 with extending irradiation time

Fig. 5(b) compares photocatalytic degradation of RBR-X3B on $La_2Ti_2O_7$ and 70%$La_2Ti_2O_7$/HZSM-5 with prolonged irradiating time. Photocatalytic degradation efficiency is 23.4% on pure $La_2Ti_2O_7$ after 120 min of illumination. Meanwhile, degradation efficiency is 79.9% on 70%$La_2Ti_2O_7$/HZSM-5 after the same irradiating time. Photocatalytic activity of 70%$La_2Ti_2O_7$/HZSM-5 is greatly improved after supporting $La_2Ti_2O_7$ on HZSM-5. $\chi La_2Ti_2O_7$/HZSM-5 has higher BET surface areas, smaller crystallite size and new mesoporous structure as compared to unsupported $La_2Ti_2O_7$.

4. Conclusions

The loading weight percentage of $La_2Ti_2O_7$ has important effects on properties of the composite $\chi La_2Ti_2O_7$/HZSM-5 photocatalyst. Surface area and total pore volume of $\chi La_2Ti_2O_7$/HZSM-5 are significantly enlarged with rising HZSM-5 content. A slight blue shift of the band edge can be seen with increasing HZSM-5 weight percent. All the binding energies of La3*d*, Ti2*p* and O1*s* electrons in $La_2Ti_2O_7$ slightly increase after loading on HZSM-5. Photocatalytic activity of 70%$La_2Ti_2O_7$/HZSM-5 is greatly improved after supporting $La_2Ti_2O_7$ on HZSM-5.

Acknowledgments

This work was supported by the Natural Science Foundation of Liaoning Province (No. 2015020186).

References

[1] M. R. Hoffmann, S. T. Martin, W. Choi, W. Bahnemann, Chem. Rev. **95**, 69 (1995).
[2] A. Fujishima, T. N. Rao, D. A. Tryk, J. Photoch. Photobio. C **1**, 121 (2000).
[3] D. Chatterjee, S. Dasgupta, J. Photoch. Photobio. C **6**, 186 (2005).
[4] K. Rajeshwar, M. E. Osugi, W. Chanmanee, C. R. Chenthamarakshan, M. V. B. Zanoni, P. Kajitvichyanukul, R. Krishnan-Ayer, J. Photoch. Photobio. C **9**, 171 (2008).
[5] G. Plantard, T. Janin, V. Goetz, S. Brosillon, Appl. Catal. B **115–116**, 38 (2012).
[6] W. J. Zhang, Y. Li, F. H. Wang, J. Mater. Sci. Technol. **18**, 101 (2002).
[7] L. Hou, G Sun, K. Liu, J. Sol-Gel Sci. Technol. **40**, 9 (2006).
[8] X. X. Fu, Q. H. Yang, J. Z. Wang, J. Rare Earths **21**, 424 (2003).
[9] C. Y. Fu, C. Chang, C. S. Hsu, Mater. Chem. Phys. **91**, 28 (2005).
[10] H. W. Eng, P. W. Barnes, B. M. Auer, M. Woodward, Solid State Chem. **175**, 94 (2003).
[11] H. Kato, A. Kudo, J. Photoch. Photobio. A **145**, 129 (2001).
[12] M. A. O'Neill, F. L. Cozens, N. P. J. Schepp, Phys. Chem. B **105**, 12746 (2001).
[13] D. Arney, B. Porter, B. Greve, P. A. Maggard, J. Photochem. Photobiol. A **199**, 230 (2008).
[14] W. M. Hou, Y. Ku, J. Alloys Compd. **509**, 5913 (2011).
[15] Z. Wang, K. Teramura, S. Hosokawa, T. Tanaka, Appl. Catal. B: Environ. **163**, 241 (2015).
[16] Y. Wang, L. Du, L. Li, W. Zhang, Optoelectron. Adv. Mat. **10**, 950 (2016).
[17] K. Onozuka, Y. Kawakami, H. Imai, T. Yokoi, T. Tatsumi, J. N. Kondo, J. Solid. State. Chem. **192**, 87 (2012).
[18] W. J. Zhang, F. F. Bi, Y. Yu, H. B. He, J. Mole. Catal. A **372**, 6 (2013).
[19] W. J. Zhang, L. Du, F. Bi, H. He, Mater. Lett. **157**, 103 (2015).
[20] L. Li, Z. Ma, F. Bi, H. Li, W. Zhang, H. He, J. Adv. Oxid. Technol. **19**, 310 (2016).
[21] P. Scherrer, Göttinger Nachrichten Gesell. **2**, 98 (1918).
[22] A. Patterson, Phys. Rev. **56**, 978 (1939).
[23] J. Tauc, R. Grigorovici, A. Vancu, Phys. Status Solidi **15**, 627 (1966).
[24] J. Tauc, Mater. Res. Bull. **3**, 37 (1968).
[25] M. Yang, L. H. Huo, H. Zhao, S. Gao, Z. M. Rong, Sensor. Actuat. B **143**, 111 (2009).
[26] J. S. Wang, M. L. Zhou, J. X. Zhang, Z. R. Nie, T. Y. Zuo, Rare Metal Mater. Eng. **29**, 335 (2000).
[27] J. Pouilleau, D. Devilliers, H. Groult, P. Marcus, J. Mater. Sci. **32**, 5645 (1997).
[28] F. Bin, C. L. Song, G Lv, J. O. Song, S. H. Wu, X. D. Li, Appl. Catal. B **150-151**, 532 (2014).

*Corresponding author: wjzhang@aliyun.com